Dynamic Properties of Na^+ Ions in Models of Ion Channels: A Molecular Dynamics Study

G. R. Smith and M. S. P. Sansom
Laboratory of Molecular Biophysics, University of Oxford, Oxford OX1 3QU, United Kingdom

ABSTRACT We present simulation results for the effective diffusion coefficients of a sodium ion in a series of model ion channels of different diameters and hydrophobicities, including models of alamethicin, a leucine-serine peptide, and the M2 helix bundle of the nicotinic acetylcholine receptor. The diffusion coefficient, which in the simulations has a value of 0.15(2) $Å^2ps^{-1}$ in bulk water, is found to be reduced to as little as 0.02(1) $Å^2ps^{-1}$ in the narrower channels, and to about 0.10(5) $Å^2ps^{-1}$ in wider channels such as the nicotinic acetylcholine receptor. It is anticipated that this work will be useful in connection with calculations of channel conductivity using such techniques as the Poisson-Nernst-Planck equation, Eyring rate theory, or Brownian dynamics.

INTRODUCTION

Ion channels are membrane proteins that allow charged particles to cross the lipid bilayer, which is normally impermeable to them. Ion channels are ubiquitous in both prokaryotic and eukaryotic cells, playing important roles in homeostasis, signaling (in excitable cells), and producing and maintaining the membrane potential that is coupled to many other transport processes. Because of the relatively simple passive nature of the ion flux through them, ion channels form an ideal field of study for attempting to gain an understanding of a simple membrane transport process.

The main source of functional information about ion channels is electrophysiology experiments from which the current-voltage (*I-V*) relations of the channels can be measured and their dependence on the concentration and chemical nature of current-carrying ions investigated (Hille, 1992). The effect of point mutations on channel conductance has also been the subject of an enormous amount of work. However, it is currently very difficult to interpret the mass of electrophysiological data that comes from mutagenesis at a structural level other than in a qualitative way.

Perhaps the fundamental goal of simulation studies of ion channels is, therefore, to understand the structure-function relationship of the channels, i.e., how the structure (assuming, for the moment, that it is known) leads to the observed electrophysiological characteristics of the channel: *I-V* curves, reversal potentials, etc. One of the best tools for making this connection is the use of computer simulation of a model of the structure. Several programs have been developed, e.g. Charmm (Brookes et al., 1983), GROMACS (http://rugmd0.chem.rug.nl/gmx/index.html), GROMOS (http://igc.ethz.ch/gromos/), and AMBER (http://www.amber.ucsf.edu/amber/amber.html), which permit simulation of complex atomistic biological systems; they use molecular dynamics (MD) to evolve the structure in time, modeling the bonded and nonbonded interactions between atoms using simple classical potentials. In the case of ion permeation, where no chemical bonds are made or re-formed, it is an acceptable approximation to use classical, rather than quantum, mechanics in all parts of the simulation.

Nevertheless, the task is still far from easy. Full atomistic simulations, even of incomplete models of ion channels, contain thousands of atoms and the time scale of the permeation of even a single ion is sufficiently long ($\sim$1 μs) that it is inaccessible to simulations of such models using existing computers; moreover, the passage of many ions, not just one, would have to be observed in practice before a reliable estimate of I as a function of V could be made. For this reason, the connection of structure to function is not fully understood even for channels whose structure is known. Of course, at the present time atomic-resolution structural information is available for only a few channels, such as gramicidin A (Urry, 1971; Wallace, 1986; Nicholson et al., 1991; Doyle and Wallace, 1997), porins (Cowan et al., 1992; Kreusch et al., 1994), pore-forming toxins (Song et al., 1996) and the *Streptomyces lividans* potassium channel (Doyle et al., 1998); the best guesses for the structures of the majority of channels are usually derived from lower-resolution structural data and indirect evidence from mutagenesis experiments.

To reach timescales of physiological interest (and also to gain real understanding), it is necessary to simplify the model by averaging some of the degrees of freedom that would not be expected to have a direct bearing on the ion permeation, such as those relating to the dynamics of the solvent or to certain parts of the protein. However, the resulting coarse-grained models of ion permeation require extra system-specific input parameters or functions that capture in some way the effect of the degrees of freedom that have been omitted; these are quantities such as the free energy of the ion as a function of its position in the channel

Received for publication February 3, 1998 and in final form June 12, 1998.
Address reprint requests to Dr. Mark S. P. Sansom, Laboratory of Molecular Biophysics, Rex Richards Building, University of Oxford, South Parks Road, Oxford OX1 3QU, U.K. Tel.: 44-1865-275371; Fax: 44-1865-275182; E-mail: mark@biop.ox.ac.uk.

0006-3495/98/12/2767/16 $2.00

(also known as the potential of mean force) or the diffusion coefficient of the ion in the channel (the focus of investigation in this paper). These parameters *can* be estimated from MD simulations which do not themselves reach the timescales of physiological ion permeation. Thus, a fairly clear program for estimating channel conductance emerges: use MD simulation of short-timescale processes to provide the parameters needed by longer-timescale simulation methods. Such hierarchies of simulation techniques have been envisaged by other workers in this field (see, e.g., Cooper et al., 1985; Chiu et al., 1993; Berne, 1985) and in the case of gramicidin implemented to some extent (Jakobsson and Chiu, 1987; Chiu and Jakobsson, 1989; Chiu et al., 1993); (Roux and Karplus, 1991b; Roux and Karplus, 1991a; Roux and Karplus, 1993). The work reported here is concerned with the first part of the program: to provide an estimate of the effective diffusion coefficient D of sodium ions in a series of model channels. Use of the estimated diffusion coefficients to calculate theoretical I-V curves that may be compared with experiment will not be undertaken here, though in the Discussion section we briefly discuss one of the methods by which conductance calculations may be carried out, the Poisson-Nernst-Planck equation (Chen et al., 1997a). This will also make clear that knowledge of D of the ion (and other properties of the ion and channel) are of great importance in such calculations.

It may not be obvious that a change in ionic diffusion coefficient in the channel environment is to be expected. However, there is already substantial evidence indicating that this is the case. In the extensive simulation work on gramicidin (Jakobsson and Chiu, 1987; Chiu and Jakobsson, 1989; Chiu et al., 1991; Roux and Karplus, 1991b; Roux and Karplus, 1991a; Chiu et al., 1993; Roux and Karplus, 1993; Roux et al., 1995), reductions of at least one order of magnitude (and possibly two) for Na^+, and at least a factor of two for K^+, have been widely reported. The various estimates that have been made are reviewed in Roux and Karplus (1991a) and are discussed below. The gramicidin channel is perhaps slightly unusual because of the extremely intimate association that occurs between ion and peptide throughout its length, but a reduction in ionic mobility has also been observed in work on mobility of ions in channel-like hydrophobic cavities (Lynden-Bell and Rasaiah, 1996), in which the channel acts by confinement only. Moreover, it is already known from simulation and experiment that the diffusion coefficient of *water* in many channels is reduced by its confinement (Gutman et al., 1992; Chiu et al., 1993; Sancho et al., 1995; Breed et al., 1996); given that the motion of a hydrated ion is coupled (though not in a simple way) to the motions of surrounding waters, it is to be expected that its motion will also be affected.

If it did become possible to predict reliable theoretical I-V curves starting from atomistic models, a state of affairs toward which this work is a step, then their agreement with experimental I-V curves would validate the model; conversely, a lack of agreement would show that the model required modification (Kienker and Lear, 1995; Chen et al., 1997b). Thus, it would become possible to use experiments as an input to the modeling process in a much more precise and qualitative way than is now possible.

METHODS

Systems studied

We have investigated various channel models, so that it will be more apparent which features of the results are particular to a particular model and which are general. Molscript (Kraulis, 1991) diagrams of the models that were studied are shown in Fig. 1. These models display a range of features: they have a range of pore diameters; four are α-helix bundles whereas one is a β-barrel; some are much simplified relative to the channels that occur in biological systems, whereas others use the sequences of (fragments of) real channels. All the models were generated following the simulated annealing by molecular dynamics (SA/MD) protocol described in previous papers (Kerr et al., 1994; Sansom et al., 1995; Sankararamakrishnan et al., 1996). In this procedure, templates for the initial positions of Cα atoms are generated according to the geometry of an ideal α-helix or β-strand, modified as necessary by available structural data, and the system is slowly allowed to relax (*in vacuo*) from an initial high temperature state in which the secondary structure is maintained by constraints but the side-chains are extremely flexible to a much less heavily constrained final state at ~300 K. The procedure is repeated to generate an ensemble of candidate structures, one of which is selected for further investigation. Water is then added from a pre-equilibrated box and an Na^+ ion is also introduced (with the deletion of a water molecule at its initial position). This system is then minimized, heated and equilibrated before each of a series of production runs from which the properties of the ion are calculated. Further details of the simulation protocol, in particular the restraints used, are given in the next subsection. All of the models were aligned with the pore axis along z, with the origin approximately at the center of the channel. The models studied were:

Control

Two cubic boxes, one containing 124 TIP3P water molecules and one Na^+ ion and having dimensions 15.6 Å × 15.6 Å × 15.6 Å, and the other containing 999 TIP3P water molecules and one Na^+ ion, and having dimensions 31.1 Å × 31.1 Å × 31.1 Å. These systems acted as controls, setting the scale for any alteration of diffusion coefficient observed in the channels themselves.

n8s8

An eight-stranded poly-Ala β-barrel model, which will be referred to as n8s8 (Fig. 1 *A*). This model served as a simple paradigm of a β-barrel. Each strand was 10 alanine residues in length and the barrel had a shear number of 8. The strands were separate, rather than being connected by loops, forming a barrel of length of about 30 Å and pore radius of about 3.5 Å. All pore radii were calculated using the HOLE program (Smart et al., 1993). The solvated system contained 293 TIP3P water molecules in total, about 100 (±5) of them in the pore and 200 in the caps. Properties of water, such as its diffusion coefficient and its response to an external electric field, have been studied previously in this model (Breed et al., 1996; Sansom et al., 1997).

an5

A five-staved poly-Ala α-helix bundle model, which will be referred to as an5, serving as a simple paradigm of a helix bundle (Fig. 1 *B*). The sequence of each helix was $(A)_{20}$. The bundle was again about 30 Å in length, with a pore radius about 2.0 Å, and when solvated contained 159

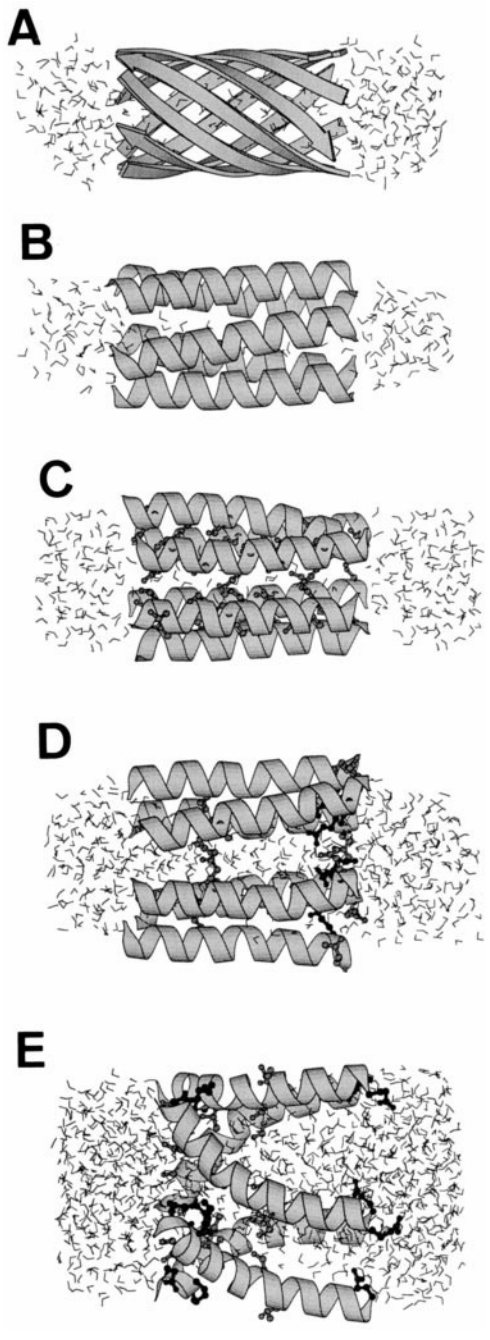

FIGURE 1 Diagrams of the various channel models investigated. (*A*) 8-stranded poly-Ala β-barrel model (n8s8); (*B*) 5-staved poly-Ala α-helix model (an5); (*C*) 6-staved Leucine-Serine peptide α-helix model (leu-ser); (*D*) 6-staved alamethicin α-helix model (alm); (*E*) $(\alpha 7)_5$ nAChR model. The secondary structural elements are shown in ribbon format, with only polar and ionizable side chains shown explicitly, and water is shown in bonds-only format.

TIP3P water molecules, about 40 ($\pm$3) of them in the pore. This model was also studied by Breed et al. (1996) and Sansom et al. (1997).

leu-ser

A six-staved α-helix model of a leucine-serine peptide, which will be referred to as leu-ser (Fig. 1 *C*). The sequence of each helix, $(LSSLLSL)_3$, was the same as that of a real, artificially synthesized leucine-serine peptide whose channel-forming properties have been extensively studied (Lear et al., 1988; Lear et al., 1994; Kienker et al., 1994; Kienker and Lear, 1995). This sequence forms amphipathic α-helices with the leucine residues on one side and the serines on the other. This peptide spontaneously forms inwardly rectifying channels in lipid bilayers, thought to consist of α-helical bundles with the serine residues lining the pore and the leucines directed toward the lipid. The number of subunits per channel has not been measured experimentally but previous modeling studies (Lear et al., 1994; Mitton and Sansom, 1996) suggest that a molecularity of six may be the most likely. The model has a length of about 30 Å, with a pore radius of about 3.5 Å in the center of the channel that falls to about 2.0 Å near the mouths. It is solvated with 250 water molecules, of which about 85 ($\pm$5) lie in the pore.

alm

A six-staved α-helix model of the channel formed by the fungal peptide alamethicin, which will be referred to as alm (Fig. 1 *D*). The sequence of each monomer is UPUAUAQUVUGLUPVUUEQ Phl, where U represents the α-amino isobutyric acid residue (i.e., $-NHC(CH_3)_2CO-$) and Phl represents the phenylalaninol residue (i.e., $-NHCH(C_6H_5)CH_2OH$). The crystal structure of the alamethicin monomer is known to atomic resolution (Fox and Richards, 1982), and there is good evidence that channels are formed from bundles containing a variable number of monomers (including six) (Woolley and Wallace, 1992; Sansom, 1993; You et al., 1996; Woolley et al., 1997), corresponding to the various conductance states of alamethicin channels (Cafiso, 1994). The hexameric bundle investigated here is one from a series of such bundles containing between 4 and 8 monomers that have been studied previously (Breed et al., 1996, 1997). The helices are kinked near the central proline residue and arranged with their hydrophilic faces (defined by Q7) facing the pore. Once again, the model has a length of about 30 Å, with a largest pore radius of about 5.2 Å just C-terminal of the center of the channel, falling to about 3.0 Å about 5 Å in from the channel mouths at each end. It is solvated with 513 water molecules, of which about 200 lie in the pore.

nAChR

A model of the putative pore-lining M2 helix bundle of the nicotinic acetylcholine receptor (nAChR) (Fig. 1 *E*). The nAChR is the best-characterized member of the superfamily of ligand-gated ion channels (Karlin and Akabas, 1995; Hucho et al., 1996); it forms pentameric cation-selective channels and is found in the nerve-muscle synapse and in the central nervous system. Of the four transmembrane segments in each subunit, the M2 segments are believed to form the majority of the lining of the pore (Hucho et al., 1986; Villarroel et al., 1991; Cohen et al., 1992; Akabas et al., 1992; Akabas et al., 1994). The model used here, which incorporates structural information deduced from cryo-EM (Unwin, 1993; Unwin, 1995) and mutagenesis (Akabas et al., 1992; Akabas et al., 1994) data, has already been the subject of MD studies (Smith and Sansom, 1997). It consists of a homopentameric bundle of centrally-kinked helices that form a loose right-handed supercoil. Each helix has the sequence EKISLGITVLLSLTVFMLLVAE; this is the sequence of the M2 segment of the neuronal α7 nAChR, which is known experimentally to form homopentameric channels, at least *in vitro* (Changeux et al., 1992; Galzi et al., 1992; Bertrand et al., 1992). The bundle is about 32 Å in length, with a minimum pore radius of $\sim$6 Å, increasing to 18 Å near the helix C-termini. It is solvated with a total of 1026 TIP3P water molecules, of which about 430 lie in the pore, and it is assumed that all ionizable residues are in their fully ionized states.

Details of simulations

All simulations were performed using the program Charmm23 (Brooks et al., 1983) running on Silicon Graphics workstations and servers and DEC

alpha AXP workstations. The param19 parameter set was used. Aliphatic groups were represented by extended carbon atoms; polar hydrogen atoms were, however, included explicitly. The water model employed was the TIP3P model, which is a three-center nonpolarizable model. Every polypeptide chain in every model was patched at the *N*-terminus by an acetyl group, and (except for alamethicin, which has a C-terminal amino alcohol) at the C-terminus by an NH_2 group, to mimic the effect of the preceding and following amino acid.

The models were minimized for 3000 steps using the adopted-basis Newton-Raphson method before starting MD. MD was performed with a 1-fs timestep and the lengths of bonds to hydrogen constrained with the SHAKE algorithm. The system was heated to 300K over 6 ps using a constant-energy scheme with periodic rescaling of molecular velocities. Then for the equilibration and production stages of the simulation we switched to the constant-temperature Nosé-Hoover method (Nosé, 1984). The equilibration stage was 19 ps long for the nAChR models, 18 ps long for the others. All production trajectories were 100 ps long and were sampled every 0.1 ps, thereby giving 1000 coordinate sets for the Na^+ ion. For each model, this procedure of minimization, heating, equilibration, and production was repeated for several (typically 11) initial release positions of the sodium ion in the channel pore and water caps.

The water was prevented from escaping from the channels by using the MMFP module of Charmm to put cylindrical or (in the case of the nAChR) hourglass-shaped restraining potentials on it. Given that there is no explicit bilayer in these simulations, and in the case of the nicotinic receptor model most of the protein is also absent, it is also necessary to use additional restraints to maintain the geometry of the models; these take the form of harmonic positional restraints put on the Cα atoms only, to keep them close to their positions in the initial SA/MD structures. (In the case of the nAChR, the Cα atoms near the center of each helix are not restrained). The force constant of the restraining potential was 10 kcal mol^{-1} $Å^{-2}$. This is a stronger potential than was generally used in the simulations on gramicidin, e.g. 0.6 kcal mol^{-1} $Å^{-2}$, in conjunction with dissipative Langevin forces, was used by Roux and Karplus (1993). In Chiu et al. (1991) it was found that holding the channel completely rigid reduced the mobility of water and ions very substantially; in later work (Chiu et al., 1993) these authors used a nonharmonic restraining potential (though this was applied to all protein atoms rather than just the Cα atoms) with relaxation times of 20–60 ps, whereas the time constant (1/(frequency of harmonic vibration)) of a 10 kcal mol^{-1} $Å^{-2}$ potential is 0.34 ps. However, in justification of our procedure, we remark that recent simulations of water in alamethicin with an explicit, hydrated lipid bilayer (Sansom, Berendsen and Tieleman, manuscript in preparation) have found a reduction in the self-diffusion coefficient of *water* that is very similar to what was observed in the present alm model, where lipid was not included (Breed et al., 1996). Moreover, simulations of water in the restrained leu-ser model used here (Breed et al., 1996) yielded dynamic properties of pore water similar to those recently observed in multinanosecond MD of a similar leu-ser model in membrane mimetic (octane/water) (Zhong et al., 1998). Taken together, these results give us confidence that useful dynamic information on the ionic diffusion coefficient may be estimated from simple simulations. In the minimization, heating, and equilibration stages of the simulation, a harmonic MMFP restraint was also placed on the *z*-coordinate of the ion to keep it near its starting position. This restraint was removed at the start of the production stage. In the case of the two water boxes, the cubic geometry was maintained with six planar MMFP restraints for consistency with the channel models; periodic boundaries were not used.

In all stages of the simulations, long-range electrostatics were cut off at 13 Å using the force-shift method; given that lipid and distant protein were omitted in these models, it was felt that little extra accuracy would be gained to outweigh the extra computational cost of including long-range interactions.

The above simulation procedure was chosen only after the investigation of several alternatives; simulations of the n8s8 and an5 models and the $(31 Å)^3$ water box were performed with normal constant-energy MD and with extended (Stote et al., 1991) as well as cut-off electrostatics. In the case of water boxes, the effect of using periodic boundary conditions was also investigated. Simulations were also done in which the ion was free to move throughout all stages of the simulation, rather than being restrained until the end of equilibration. The results of these tests are reported in appendix B; generally the protocol does not seem to affect the results, within the error bars.

Calculation of effective diffusion coefficient *D*

Our approach to calculating *D* is similar to that used in Chiu et al. (1993) for gramicidin; we use the equation

$$D = \lim_{t\to\infty} \langle (r - \langle r \rangle)^2 \rangle / 2dt \tag{1}$$

where t is the time, $\langle (r - \langle r \rangle)^2 \rangle$ the mean squared displacement from the mean and d the spatial dimension. This is a slightly modified version of the standard approach, where $D = \lim_{t\to\infty} \langle r^2 \rangle / 2dt$ is used. The $\langle r \rangle$ correction was introduced because it was thought that there might be an appreciable deviation from simple diffusive motion even at fairly short times, from a uniform drift motion due to interaction with the helix dipoles; Eq. 1 reduces to the usual form if there is no net drift, but also gives an unbiased estimate of D in the case of a uniform drift (where using $\langle r^2 \rangle / 2dt$ overestimates D). This was confirmed by tests on simple random-walk trajectories with and without drift generated by a Monte Carlo procedure in which D was an input parameter. In fact, in the ion channel models themselves, the correction made a negligible difference in all but a few cases. The formal $\lim_{t\to\infty}$ corresponds in practice to fitting the gradient of $\langle (r - \langle r \rangle)^2 \rangle$ vs. t for fairly *short* times (we used the interval 1–6 ps, chosen on the basis of inspection of the measured graphs of $\langle (z - \langle z \rangle)^2 \rangle$ vs. t, examples of which are shown in Fig. 2 *D*). The expectation value $\langle \cdot \rangle$ is approximated by the average over all the pairs of points in the trajectory that are separated by time t. The size of the error bars was estimated from a jackknife blocking technique (Grey and Schucany, 1972), in which the trajectory was divided into N_b blocks and D estimated N_b times, the ith estimator D_i coming from all the data *except* the ith block. The error (the standard error of the mean) is then given by $\sqrt{(N_b - 1)var(\{D_i\})}$.

The trajectories used were sufficiently short that in most cases the ion did not move very far from its starting point, so that the D measured is a spatially local quantity, $D(\boldsymbol{r})$, where the $\boldsymbol{r}$ is defined as the average coordinate of the ion. At least with respect to the narrow channels, it is natural to consider this as a function of z only, $D(z)$, where z is the average z-coordinate of the ion). In a few cases, the ion was seen to move in such a way that it seemed to be in different diffusion regimes in different parts of the trajectory. In these cases, the trajectory was subdivided and only the segments lying in a particular region of space were used when calculating the estimate of $D(\boldsymbol{r})$ there.

It is natural in the case of a homogeneous system to consider the motion in all three spatial dimensions and estimate

$$D \equiv D_r = \lim_{t\to\infty} \langle (r - \langle r \rangle)^2 \rangle / 6t \tag{2}$$

with $r^2 = x^2 + y^2 + z^2$; this equation was used in estimating D in the two water boxes, for example. However, for ions in the channel models we shall consider the motions along the channel (z) axis and perpendicular to it separately, as the character of these motions is likely to be different. Therefore, we define

$$D_\parallel = \lim_{t\to\infty} \langle (z - \langle z \rangle)^2 \rangle / 2t \tag{3}$$

and

$$D_\perp = \lim_{t\to\infty} (\langle (x - \langle x \rangle)^2 \rangle + \langle (y - \langle y \rangle)^2 \rangle) / 4t. \tag{4}$$

An additional consideration in analyzing the diffusion is the fact that (even in bulk solution or molecular liquids) $\langle r^2 \rangle$ vs t has a shoulder between an initial steep rate of increase, where the ion can be thought of as moving

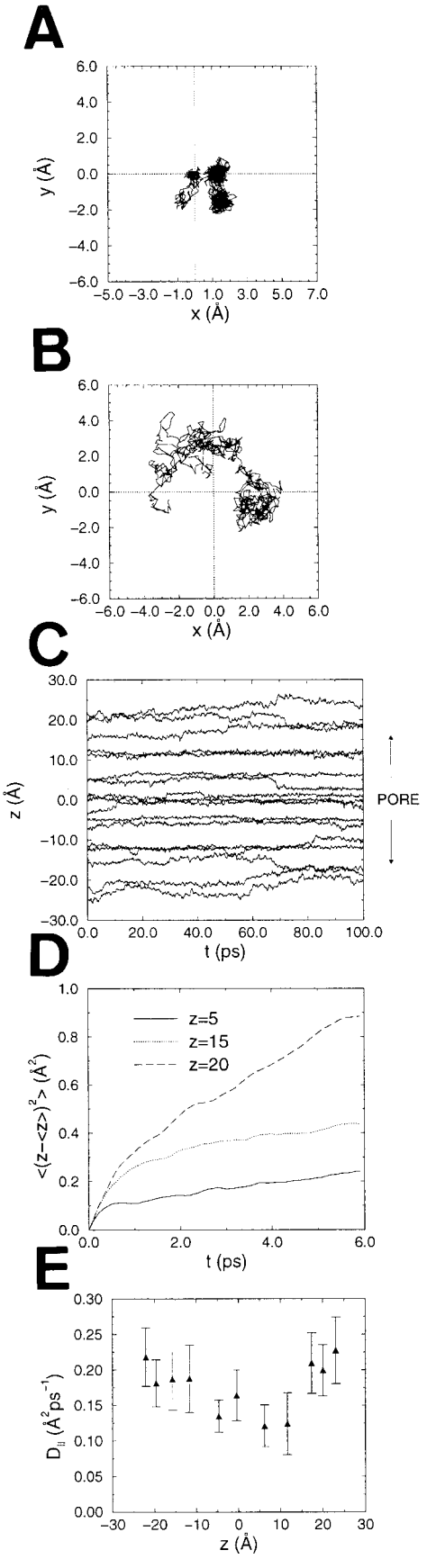

FIGURE 2 Representative ion trajectories and graphs of $\langle(z - \langle z\rangle)^2\rangle$ vs. t for the n8s8 model. (*A*) the $(x - y)$ trajectory of the ion at $z = 5$ (near the center of the channel); (*B*) the $(x - y)$ trajectory of the ion at $z = 20$ (in the water cap); (*C*) z-coordinates of the ion vs. time t; (*D*) $\langle(z - \langle z\rangle)^2\rangle$ vs. t for various positions of the ion; (*E*) local or fluid dynamic diffusion coefficient $\mathcal{D}$ from motion in the z-direction as a function of average z-position of the ion, estimated by fitting the gradient of $\langle(z - \langle z\rangle)^2\rangle$ vs. t between 0.1 and 0.5 ps.

within the (dynamic) cage formed by its first solvation shell, and a slower long-time increase, which is the normal diffusion coefficient as defined above, and which corresponds to the ion escaping from this dynamic cage. If the initial rate of increase of mean squared displacement with time is fitted (i.e. 0.1–0.5 ps rather than 1–6 ps), the result is the local, or cage, or fluid dynamic "diffusion coefficient" $\mathcal{D}$ (we place the words "diffusion coefficient" in quotes because, on such a short time scale, the motion is strongly inertial rather than properly diffusive).

The justification for using the mean squared displacement approach depends on a separation of length (or time) scales in the motion of the ion in the channel. On very short length scales, where the motion corresponds to $\mathcal{D}$, one would not expect a large difference between the motion in a channel and in bulk solution, and this has been confirmed by the simulations on gramicidin (Chiu et al., 1993). Conversely, on sufficiently large length scales, the motion will be heavily influenced by the energy gradients produced by the channel protein, which would tend to reduce the rate of increase of $\langle(r - \langle r\rangle)^2\rangle$ with t by creating potential wells and barriers that must be crossed. Let us denote the gradient of the electrostatic energy of the ion due to the channel protein by $\nabla\Phi_{ch}$. Our hope, then, is that there is an lengthy intermediate regime, of length scale up to L say, where $\nabla\Phi_{ch}$ is relatively constant and the deviation of D of the ion from its bulk-solution value is due mainly to the fact that it and its surrounding waters are physically constrained. This D would then be the effective diffusion coefficient that it would be appropriate to use, in combination with a knowledge of Φ_{ch}, or the position-dependent free energy (potential of mean force), in conductance calculations. We shall return the method of estimation of D and compare it with some of the others that have been adopted in the Discussion section.

Finally, we remark that, in the case of the an5 channel, the ion trajectory seemed to show a different kind of diffusion to that seen in the other channels; the ion was almost stationary in z for long periods, but made occasional large jumps of roughly constant size, approximately 2 Å. The number of such jumps during a particular trajectory was usually small. Though Eq. 1 should still be appropriate to analyze this motion, we have in this case compared the results of Eq. 1 with those of a Bayesian approach, described in appendix A. The estimates of D derived by this method agree with those from Eq. 1 within the error bars.

RESULTS

Diffusion near the center of the channel

We first describe the diffusive motion that was observed when the ion was initially placed on the channel axis, i.e., at the point (0, 0, z_i) for $z_i = \{-20, -15, -10, -5, 0, 5, 10, 15, 20\}$ Å. For most models, extra runs were done with the ion starting at other points, e.g., at $z_i = \{-25, -13, -8, -3, 2, 7, 12, 25\}$ Å for an5. In Fig. 2, *A* and *B*, we show the ion trajectories in the (x, y)-plane, i.e., perpendicular to the channel axis, for representative points in the cap and in the channel pore for the n8s8 model. Fig. 2 *C* shows the z-coordinate of the ion as a function of time for all the release points in this model. The greater mobility in the caps compared to the pore is qualitatively apparent from examination of these trajectories alone, and is reflected in the corresponding graphs of $\langle(z - \langle z\rangle)^2\rangle$ vs t (Fig. 2 *D*), from

which D is calculated. As anticipated there is an initial rapid increase in $\langle(z - \langle z\rangle)^2\rangle$, largely independent of position in the channel and corresponding to diffusion within a cage of solvating water molecules, followed by a rather slower increase corresponding to the desired intermediate regime of diffusion; the gradient of this part of the graph is clearly much lower in the channel proper than in the water caps. We have also calculated the short-time local fluid dynamic diffusion coefficient $\mathcal{D}$ from z-displacement between 0 and 0.5 ps (Fig. 2 *E*). $\mathcal{D}$ is much larger ($\sim$0.20 Å^2 ps^{-1}, approximately equal to $\sim$0.18 Å^2 ps^{-1} reported in Chiu et al. (1991)) than the long-time effective D, and although it does decrease slightly in the channel pore, the decrease is proportionately much smaller than for the corresponding effective diffusion coefficient $D_\parallel$ (Fig. 3 *A*), which we discuss next.

The estimates of $D_\parallel$ were calculated from z-displacement only, according to Eq. 3, fitted between 1 and 6 ps. They are shown for the various channels in Fig. 3. For comparison, in the simulations on the ions in the two water boxes of different sizes, it was found that $D = 0.11(3)$ Å^2 ps^{-1} for $L = 15.5$ Å and $D = 0.15(2)$ Å^2 ps^{-1} for $L = 31$ Å. The error bars on the channel simulations are quite large, but there is a very clear reduction in D in the pore regions of the an5 and n8s8 models, to only about $D \approx 0.02$–0.04 Å^2 ps^{-1}, compared with $D \approx 0.08$ Å^2 ps^{-1} in the caps.

In the leu-ser model, there is a similarly pronounced reduction in the C-terminal (+ve z) half of the channel but a smaller reduction in the N-terminal half, where $D_\parallel$ seems to be about two-thirds of its value in the caps. In the alm model, the reduction seems to follow the radius profile of the channel quite closely; it is largest near the mouths (where $D_\parallel$ is reduced by 50%), whereas near $z = 5$, where not only is the channel quite wide but the charged ring of glutamate sidechains is within a few Å of the ion, $D_\parallel$ is as large as it is in the caps. The ion tends to move quickly out of the narrowest region of the channel, around $z = -5$, so no estimate of D is obtained there. Even in the relatively wide nAChR, $D_\parallel$ falls to about 0.06 Å^2 ps^{-1} in the N-terminal half of the channel, about ½ of its value in the caps ($D \approx 0.12$ Å^2 ps^{-1}, though the variation is large); its behavior in the C-terminal half is less clear-cut. This is consistent with the pore radius profile of the nAChR model, which is narrowest (radius $\approx$ 6 Å) in the *N*-terminal half and widest (radius $>$ 8 Å) in the C-terminal half.

The points which fit this general interpretation least well are those coming from just inside the *N*-terminus of the an5 model, where the estimate of $D_\parallel$ is unexpectedly large. There are two possible reasons for this. First, one would expect a strong repulsive interaction between the positive Na^+ ion and the nearby partial positive charges at the ends of the helices, which, in this very narrow channel, are close to the ion. Thus, the assumption that $\nabla\Phi_{ch}$ should be roughly constant on the scale of the ion's motion is less likely to be correct here than in any other channel, so it is difficult to separate the effects of Φ_{ch} from those of true variation in D. Second, it seems plausible that the most pronounced reduction in $D_\parallel$ should be seen only near the center of the channel, where there are several surrounding shells of water that are also in the channel proper. If the ion is near the mouths of the pore, water on one side of it will be in the caps and will not itself be restricted in its movements. There is some indication of similar behavior near the mouths of some of the other channels, though not, for example, in alm; but here the channel is narrowest near the mouths and it may be that the pronounced confinement outweighs competing effects.

As well as using z-displacement only, we have also calculated D from the displacement in the (x, y)-plane, i.e., $D_\perp$ (Eq. 4). The results are shown in Fig. 4. For the n8s8, leu-ser, alm, and nAChR models, this is comparable with $D_\parallel$ in the channel proper, though $D_\perp$ is more clearly reduced in the channel and tends to decrease more rapidly as soon as the channel is entered. Only in the case of an5 is $D_\perp$ much smaller than $D_\parallel$ for the timescales studied, as might be expected for this very narrow channel. $D_\perp$ is generally larger than $D_\parallel$ in the caps, where the latter may well be reduced by the effects of the restraining potentials put on the water.

In the case of the channel of the an5 model, as we have said, the trajectory of z vs. t was qualitatively different from that seen in other models; changes in z tended to occur only as occasional large jumps of approximately constant size. We have analyzed these trajectories using a Bayesian approach (Eqs. 8 and 9 in appendix A) and find that, for the trajectories started with $-10 \le z \le 15$, $D_\parallel$ is found to be between 0.01(1) and 0.06(4) Å^2 ps^{-1}, with an average of 0.035 Å^2 ps^{-1}. This is in reasonable agreement with the results from $\langle(z - \langle z\rangle)^2\rangle$.

It is notable that D does not generally attain the same value in the caps of the an5, n8s8 and leu-ser models as it does in the caps of alm model or the nAChR (this is more apparent from $D_\perp$ than $D_\parallel$). This is attributable to the larger size of the caps in the nAChR model; their radius is about 18 Å for the nAChR, 12 Å for leu-ser, and less than 10 Å for the others. Thus, it is entirely consistent that D should have about the same value in the wider parts of the pore of the nAChR as in the caps of the other models. The result is also consistent with the smaller D recorded in the smaller of the two water boxes, and with the finding of Lynden-Bell and Rasaiah (1996) that the diffusion coefficient of sodium in a hydrophobic cavity of radius 6 Å is 2/3 of its bulk value.

Finally, in Fig. 5 we show the diffusion coefficient from these on-axis runs as a function of the local HOLE radius of the channel. Though there is some scatter, it is fairly clear that D increases with r from very small values around $r = 2$ Å until it has reached its bulk value by about $r = 10$–12 Å. The small-r part of this figure is consistent with the results of Lynden-Bell and Rasaiah (1996). The trend is visible in $D_\parallel$ (Fig. 5 *A*), but the presence of a few outlying points, generally those corresponding to z near the mouths of the narrow channels, obscure it somewhat. The trend is clearer when D_r (Eq. 2) is considered, to take into account both $D_\parallel$ and $D_\perp$ (Fig. 5 *B*).

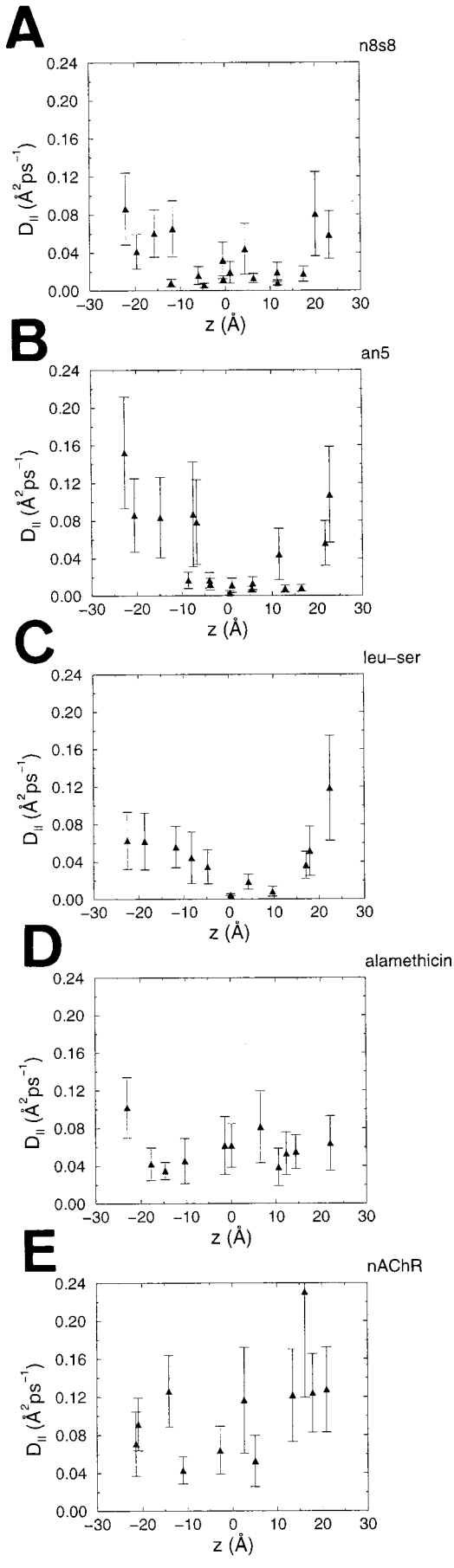

Diffusion near the channel surface in the nAChR

We have also investigated the mobility of the ion when released from points near the surface of the nAChR, to see if there is any evidence for a radially varying D in this much larger channel. In previous investigations of the behavior of water in the nAChR model pore (Smith and Sansom, 1997), it was found that the local density of water oxygen atoms could be very much higher (more than threefold higher) than the average at various positions near the protein surface, particularly at points near charged or polar sidechains. Seven of these points were chosen as release points of the Na^+ ions, as it seemed plausible that the reduction in water mobility would result in a reduction in ionic mobility too (Though in fact, the initial release points often failed to correspond to areas where the ion was content to sit; the ions regularly moved several Å during the equilibration part of the trajectory). Interpretation of the results in this case is made more difficult by the fact that the motion is to some extent one of diffusion across fixed potential barriers; by choosing release points near charged sidechains, we cannot avoid encountering the undesirable situation of $\nabla\Phi_{ch}$ varying relatively rapidly. This is demonstrated by the diffusion in the (x, y)-plane of the ion shown in Fig. 6 *A*: the motion clearly has an initial phase where the ion moves less freely than in the second half, where it escapes from the protein surface and moves into the channel. For some other release points, the opposite type of motion is observed: initial relatively free motion followed by a fall into a different potential well than the one from which the ion was released (Fig. 6 *B*). Accordingly, in analyzing D, the trajectory was divided into two according to $\rho = \sqrt{x^2 + y^2}$; if ρ was within a few angstroms of the HOLE radius of the channel at that point, the segment of the trajectory was put into one class, if it was smaller than this it was put into the other. $D_{\|}$ was calculated separately for each. The results are shown in Fig. 6 *C*. The diffusion coefficient is clearly smaller close to the protein surface than it is near the channel center, where it is comparable with the values calculated from the trajectories with the ions released on the axis (Fig. 3 *E*). Thus, aside from the reduction of D even on the channel axis of the nAChR, there is evidence that it is still further reduced if the ion approaches the channel surface. This may in some measure account for the fact that the diameter of the pore as estimated from blocking experiments (Dwyer et al., 1980; Villarroel et al., 1991; Nutter and Adams, 1995) tends to be smaller than the diameter indicated by structural studies.

Interaction with the channel surface

We have also investigated the nature of the interaction between the ion and the channel in the various channel

FIGURE 3 Diffusion coefficient from motion in the z-direction, $D_{\|}$, as a function of average z-position of the ion for (*A*) n8s8, (*B*) an5, (*C*) leu-ser, (*D*) alm, and (*E*) nAChR, estimated by fitting the gradient of $\langle(z - \langle z\rangle)^2\rangle$ vs. t between 2 and 6 ps for ions placed initially on the channel axis, at various points along it.

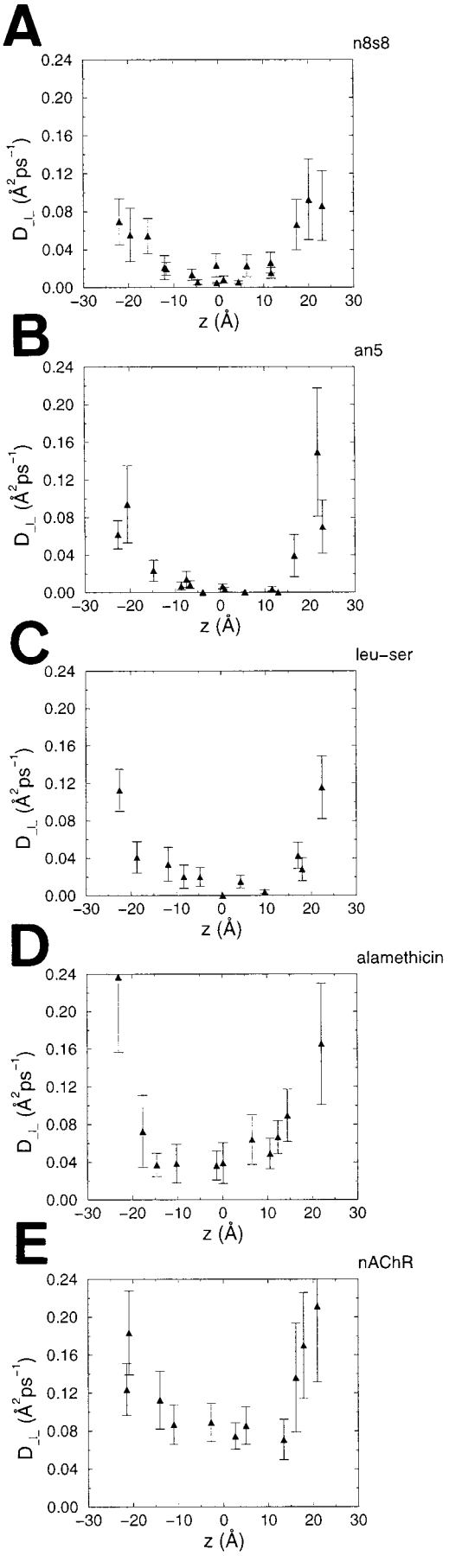

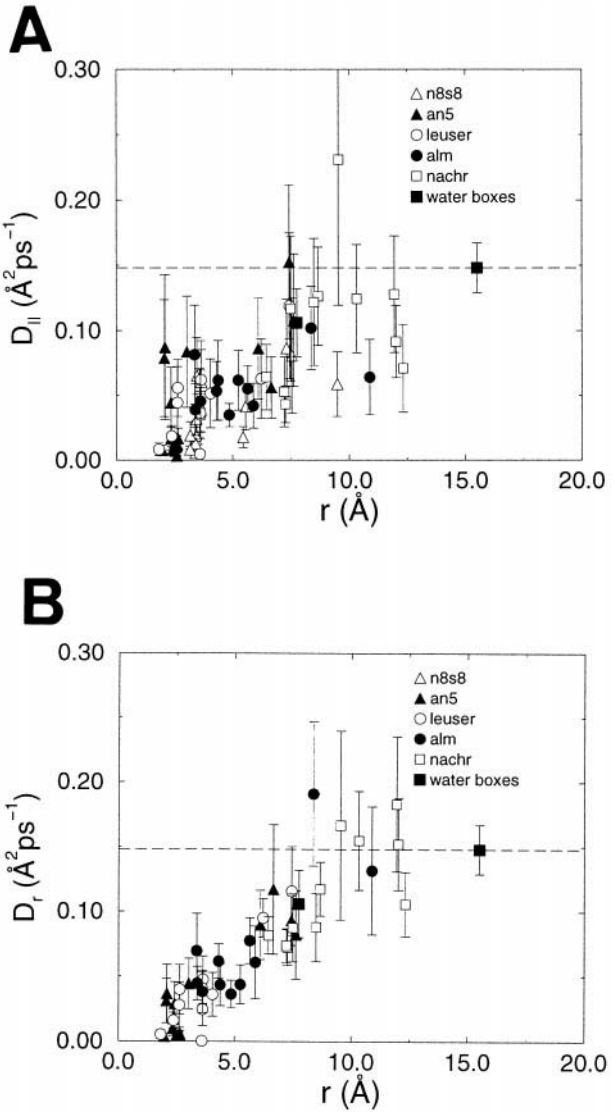

FIGURE 5 Diffusion coefficient D for the various models shown as a function of the radius r of the channel at the average z-coordinate of the ion. For comparison we also show D for the various cubic water boxes; in this case, the abscissa is half the side length of the simulation box. (A) $D_{\parallel}$; (B) D_r.

models, by calculating the radial distribution function $g(r)$ between the Na^+ ion and the protein sidechain atoms (Fig. 7). The normal definition (number of atoms in narrow shell at r from ion)/(number of ideal gas atoms of same density in shell at r)) is slightly problematic because the density of the protein is not well defined. Therefore we calculated N_a = (number of protein atoms in narrow shell at r from ion) and N_b = (number of protein atoms in shell at r from ion after ion has undergone a random displacement uniform in (−5 Å . . . 5 Å)). Then we used N_a/N_b as an estimate of $g(r)$. The

FIGURE 4 Diffusion coefficient from motion perpendicular to the pore axis, $D_{\perp}$, as a function of average z-position of the ion, for (*A*) n8s8, (*B*) an5, (*C*) leu-ser, (*D*) alm, and (*E*) nAChR.

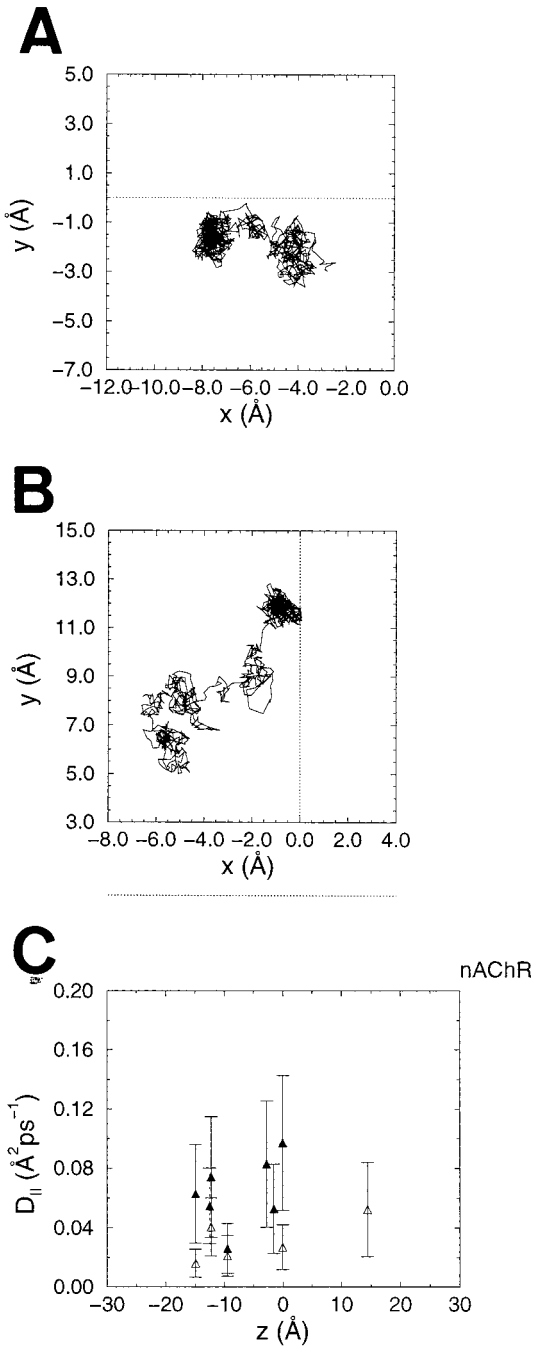

FIGURE 6 Diffusive motion of the ion in the (x, y) plane when released from positions initially close to the protein surface in the nAChR. In (*A*) we show the trajectory with the ion at $(-7.5, -1.5, -8.5)$ at the start of the production part of the trajectory; in (*B*) the trajectory with the ion at $(-5.2, 5.3, -14.5)$ initially. In (*C*) the diffusion coefficient $D_{\|}$ is calculated from parts of the trajectory near the protein surface *(open symbols)* and near the channel axis *(filled symbols)*.

random displacement decorrelates the ion from the protein, but its size, of the same order as the channel radius, ensures that on average about the same number of protein atoms will be found in total. It is clear from the results that the ion can approach the sidechains in leu-ser (Fig. 7 *C*) and alm (Fig. 7 *D*) to within 2 Å, corresponding to direct contact between ion and oxygen atoms in the sidechains (it is less than the sum of the van der Waals radii by more than 1 Å), whereas for the an5 and n8s8 channels the figure is 3 Å, comparable with the sum of the van der Waals radii, suggesting that the first solvation shell of waters around the ion is maintained at almost all times. These results are for the trajectories with the ion released at $z = 0$, but the radius at which $g(r)$ goes to zero does not depend very much on z for a given type of channel. This interpretation in terms of direct or water-mediated interaction with the channel walls is confirmed by inspection of 'snapshots' from the trajectories, and is in broad agreement with the results of Lynden-Bell and Rasaiah (1996), who observed ions approach to within 2 Å of the hydrophobic wall of a cylindrical channel; this corresponds closely to a zero of $g(r)$ at ≥ 3 Å in the channel models (because in Lynden-Bell and Rasaiah (1996), there is of course no contribution to the van der Waals radius from the channel wall of a simple hydrophobic cavity), and thus to the results found in the hydrophobic channels an5 and n8s8. In Fig. 7 *E*, $g(r)$ is shown for the ion released close to the wall of the nAChR at $z = -8$, in a hydrophilic part of the channel near to a ring of Thr sidechains; once again, it can interact directly with sidechain atoms. The general behavior shown here, direct unmediated interaction between ions and sidechains, is what would be expected to be necessary if polar sidechains play an important part in ion selectivity, as has been suggested for leu-ser and the nAChR (Bertrand et al., 1992; Galzi et al., 1992; Villarroel et al., 1991). It would not be so necessary for charged sidechains, where the electrostatic interactions are longer-range.

The behavior of $g(r)$ at larger r is also interesting. It has some structure in all the channels and, in the an5 channel, it even drops to zero after its first peak. If the ion were diffusing freely in z, this zero would not be observed; its presence confirms that in the an5 channel, as in gramicidin (the paradigm of a narrow channel), there are clear local minima of potential along the axis between which jumps are rare. Similar features, though not so well defined, can be observed in the other channels, seeming to show the presence of potential wells in the channel into which the ion is attracted.

We have also considered the $\tilde{g}(r)$ between the ion and protein *backbone* atoms (data not shown). There is much less variation in the shape of $\tilde{g}(r)$ between the different models than in the shape of $\tilde{g}(r)$. The most important feature of $\tilde{g}(r)$ is that it goes to zero at about 3.5 Å for all the helix-bundle models, and at about 4.5 Å for the n8s8 model, for all positions of the ion within the channel. Thus it does not appear that there is direct interaction between the ion and the backbone in any channel, in contrast to the case of gramicidin, where coordination of the ion by backbone carbonyl groups is known to occur (Roux and Karplus, 1991b; Roux and Karplus, 1994; Roux, 1995) and to be extremely important in the mechanism of permeation. In all the channels studied here, the sidechains form the lining of the channel. We remark that this provides further justifica-

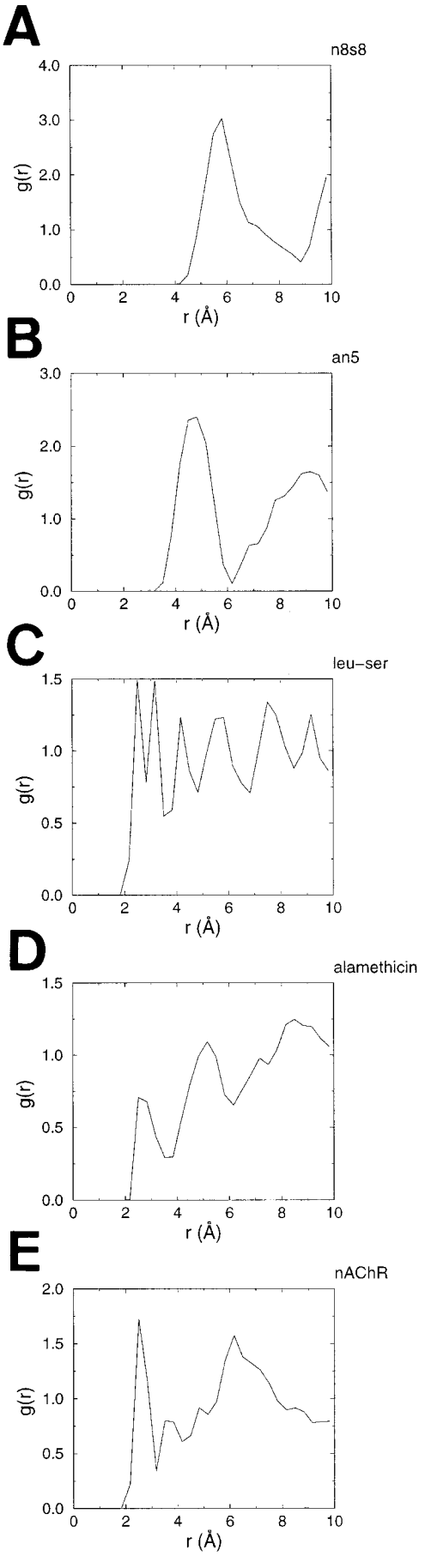

tion of the use of structural restraints on the backbone atoms: the absence of direct interaction with the ion means that any reduction in their freedom of movement will have little effect on the ion's own motion.

DISCUSSION

Models and simulation techniques

We first comment on the likely validity of the structures of those models that represent real channels (i.e. Alm, leu-ser and nAChR). The alm model is likely to be accurate at the single-helix level, given the x-ray structure (Fox and Richards, 1982) and the strong helix-forming propensity of α-amino isobutyric acid; the possibility of forming a hexameric channel seems high given the conductance states observed experimentally in channels formed of alamethicin monomers and covalently linked dimers (You et al., 1996) and the reasonable agreement of these with the estimated conductance of a hexameric bundle (Smart et al., 1997). The leu-ser model is plausible given that this peptide was *designed* to form amphipathic helices, which would then associate to form channels with a hydrophilic lining and hydrophobic exterior. The nAChR model must be counted speculative in the absence of an x-ray structure, but it is in agreement with most existing mutagenesis and cryo-EM (Unwin, 1993; Unwin, 1995) data. Other putative structures that have recently been proposed for the M2 helix bundle (Ortells and Lunt, 1996; Tikhonov and Zhorov, 1998) show reasonable agreement with the model used here. We assumed that all ionizable residues in the nAChR model were in their fully ionized states, even though very recent results (Adcock et al., 1998) suggest this may not be the case for the C-terminal glutamate ring. Further work may be necessary to establish the effect of this on D.

The most obvious omissions in the present models are those of non-pore-lining channel protein (in the nAChR), the lipid bilayer itself, and other ions which would produce a transmembrane potential difference. The effect of these omitted elements in holding the pore-lining protein in place is modeled by the use of restraining potentials. We believe that the ionic diffusion coefficient, being the result mainly of local rearrangements in the fluid involving collisions between the ion and water molecules or protein sidechains very close to it, is unlikely to be much affected by distant atoms. This would not necessarily be the case with, for example, the energetics of the ion. Thus, despite the effect of channel rigidity on permeation in gramicidin found by Chiu et al. (1991), we do not consider it necessary to incur the vastly greater computational expense of performing the simulations with these missing elements included and long range electrostatic forces taken into account, particularly when, as in the case of the nAChR, the structure of the

FIGURE 7 Radial distribution function $g(r)$ between the ion (near $z = 0$) and protein sidechain atoms for (*A*) n8s8, (*B*) an5, (*C*) leu-ser, (*D*) alm, and (*E*) nAChR (ion off-axis).

missing elements is known only in the most approximate way. This hypothesis is supported by the results for diffusion coefficient of water in the models described above, and by the fact that the backbone atoms on which the restraints are placed do not interact directly with the ion (see "Interaction with the channel surface" above).

Similar arguments justify our neglect of the transmembrane potential, which, although it is responsible for the net flux of ions through the channel at a rate of ~1 per μs, produces at any given moment a very small force compared to the jostling of nearby water molecules and thus would not be expected to have a visible effect on the diffusive motions we are studying here on a timescale about 10^4 times shorter than that of ion permeation. For example, the difference in ionic concentrations that produces the transmembrane potential corresponds to a difference of less than one in the number of ions in the water caps on the two sides of the channel in simulations of the size considered here.

Aside from structural details of the channels, it is also necessary to examine the validity of some of the simulation techniques. We have checked explicitly (appendix B) that the precise protocol used in the MD simulations (constant temperature cf. constant energy, etc.) does not appreciably affect the results. As has been suggested (Chen et al., 1997b), the use of an equilibrium simulation method to investigate a nonequilibrium steady-state process is in some ways unsatisfactory. However, we consider that this case is one in which the relaxation of the nonequilibrium part of the system is so much slower than the timescale of other motions that it will occur against a background in which the rest of the system remains effectively in equilibrium—which is really just another way of saying what we have already said in justifying the neglect of the transmembrane potential (Keizer, 1987).

Estimation of *D*

In previous work on gramicidin (Jakobsson and Chiu, 1987; Chiu and Jakobsson, 1989; Chiu et al., 1991; Roux and Karplus, 1991b; Roux and Karplus, 1991a; Chiu et al., 1993; Roux and Karplus, 1993; Roux et al., 1995), methods involving estimation of D not only from mean squared displacement but also from the autocorrelation functions of the velocity of the ion (Green-Kubo relation) and of the force on the ion when it is fixed have been used:

$$C_v = \langle (v(0) - \langle v \rangle)(v(t) - \langle v \rangle) \rangle$$

$$D = \int_0^\infty C_v dt$$

$$C_F = \langle (F(0) - \langle F \rangle)(F(t) - \langle F \rangle) \rangle$$

$$\xi = (k_B T)^{-1} \int_0^\infty C_F dt$$

$$D = (k_B T/\xi) \langle \exp(G^\ddagger/k_B T) \rangle^{-1} \langle \exp(-G^\ddagger/k_B T) \rangle^{-1}$$

where ξ is the friction coefficient and $G^\ddagger$ is the potential of mean force. The use of C_v, particularly, is a well-established alternative to mean squared displacement, but must be applied with care because the decay of C_v as t increases is not a simple exponential in dense liquids; it has been established that multiple collisions transmitting forces back to the original particle produce a power-law decay of C_v at long times (vortex diffusion) which makes the accurate numerical evaluation of its integral difficult (Alder and Wainwright, 1970; Cohen, 1993; Allen and Tildesley, 1987; Chiu et al., 1991). It is, therefore, not necessarily the case that D may be estimated from a shorter time interval using C_v than $\langle (r - \langle r \rangle)^2 \rangle$. As well as methods based on the measurement of fluctuations, measurement of D from the response to an external perturbation (using $D = k_B T \mu$, where μ is the mobility) has been used (Skerra and Brickmann, 1987). Another method is activated dynamics (Roux and Karplus, 1991a):

$$k = \kappa \langle v \theta(v) \rangle \exp(-G^\ddagger/k_B T) \Big/ \int_0^L \exp(-G^\ddagger/k_B T) dx$$

$$D = k \Delta L^2$$

where $G^\ddagger$ the potential of mean force across the fundamental (single-turn) barrier of width ΔL, and κ is the transmission coefficient, measured from trajectories initiated at the top of the barrier and propagated forward and backward; this improves the sampling of barrier-crossing trajectories. The results produced by the various methods are reviewed in Roux and Karplus (1991a).

The question of exactly what the effective diffusion coefficient *is* must also be addressed, because here there may be some differences between the gramicidin literature and the present work. On any length scale so long that the motion is diffusive (dominated by multiple randomizing collisions) rather than ballistic, it becomes possible to define an effective diffusion coefficient for motion on that scale; for instance, one could consider motion on the scale of the entire channel (length L) and define

$$D_L^{(\mathrm{eff})} = L^2/2\tau_L$$

where τ_L is the mean passage time; here, all the effect of local potential barriers is subsumed into $D_L^{(\mathrm{eff})}$. This equation is used in Roux and Karplus (1991a) to give an experimental effective D, where τ_L can be estimated from the experimental permeability; it is of little help, however, if τ_L is what we want to *predict.* Alternatively, if the channel architecture is such that there are a series of potential barriers of approximately equal height, one can define a $D^{(\mathrm{eff})}$ for crossing one of them. This is the natural approach taken in the gramicidin simulations, where the contributions of water and channel to the diffusion coefficient are comparable because the ion is coordinated by both: the potential barriers are produced by the $\Delta L \sim 1.5$ Å pitch of the β-helix, and the

quantity estimated is $D_{\Delta L}^{(eff)}$ for crossing one. The details will not be discussed here but are complicated by non-negligible inertial effects at the barrier tops. The motion through the whole channel can then be analyzed as a random walk modulated by effects with a much slower spatial variation: the access resistance, and possibly (Chiu et al., 1993) the effect of a wide central potential maximum (Jordan, 1982) that may be produced by an image potential interaction, though direct simulations have not found such a maximum (Roux and Karplus, 1993). The final results for conductance, at least for sodium, are in reasonable agreement with experiment. Results for other ions are not as good.

However, the gramicidin channel is rather unusual in that the ion is largely desolvated and coordinated instead by backbone carbonyls for most of the way down the channel. In most channels, such intimate association between ion and protein seems likely either to be confined to a relatively short stretch of the channel (for example the selectivity filter of the potassium channel (Doyle et al., 1998)) or not to occur at all; this is the case with the wider and less ion-selective channels studied here.

This difference in architecture underlies the idea, outlined in the introduction, of seeking to estimate an effective diffusion coefficient that could be used in a simplified model that no longer included water explicitly but in which a potential of mean force took account of its mean effect (and that of the protein) on the ion, and the effective D took account of the water's driving effect, and *only* of this effect, so that, in contrast with the simulations on gramicidin, the effect of the potential barriers due to the channel would not enter D. Any difference between D in the bulk and in the channel would then come from the confinement (and, in some cases, from the orientation) of water in the channel; the water produces a local potential well at the ion's present position which must relax before the ion can move any appreciable distance. The extent of the water's confinement will influence this relaxation and thus the ion's ability to move. This was our motivation for attempting to study the intermediate regime of diffusion referred to in the Methods section, where diffusion should be dominated by water confinement effects rather than those of crossing protein potential barriers. Whether this regime exists clearly depends on the structure of the channel; in narrow channels, $\nabla\Phi_{ch}$ will vary more rapidly and so the intermediate diffusive regime will become shorter. Indeed, perhaps the most serious disadvantage of having chosen to measure D from mean squared displacement is that it does not facilitate a clean separation of effects due to water from those due to protein. A method based on forces, which could of course be decomposed into contributions from water and protein, might have been advantageous in this respect.

Nevertheless, several indirect justifications for this have been found here—the concentration on relatively short time scales (up to 6 ps), the similarities of results from different channels, the similarities with diffusion in hydrophobic cavities, the lack of direct ion-channel interactions—and so our approach seems to be justified *a posteriori* for most of the channel models investigated here; however, the ultimate validation of the approach will come only after the conductance calculations have been done, which will require the potential of mean force of the ion to have been measured. It may be that the results presented here will then need to be reinterpreted as diffusion including the effect of channel potential barriers, and further simulations, together with the examination of the free energy barriers themselves, may be required to elucidate these effects fully.

The choice of water model used (TIP3P) may also affect the measured diffusion coefficient. Water's properties are, of course, unique and extremely complex for such a simple molecule, and no existing simple model (i.e., sufficiently simple to be used in an MD simulation without incurring enormous computational cost) captures them all.

Interpreting the results

In light of what we have just said about the diffusion coefficient of Na^+ in TIP3P water, we believe the results presented here should be interpreted in terms of the fractional difference between channel and bulk environments rather than as absolute values. We find that $D \approx 0.15$ Å^2 ps^{-1} for sodium in bulk solvent, compared to the experimental value of $D = 0.133$ Å^2 ps^{-1}. Thus, the reduction seen in the simulations in D to $\sim$0.1 Å^2 ps^{-1} in the nAChR channel implies that the best estimate of D of sodium in the real nAChR is 0.09 Å^2 ps^{-1} ($=0.1 \times 0.133/0.15$), and so forth. Similarly, the fractional rather than absolute changes in D are what should be considered when comparing this work with that of Lynden-Bell and Rasaiah (1996), in which the SPC/E model of water was used; the diffusion coefficient of sodium in bulk SPC/E is 0.12 Å^2 ps^{-1}. Given this, quantitative agreement between that work and our own is good. The reduction in D of the ion is similar to, though smaller than, what has been observed for the diffusion coefficient of water in channels (Gutman et al., 1992; Chiu et al., 1993; Sancho et al., 1995; Breed et al., 1996; Smith and Sansom, 1997).

In comparison with the simulations on gramicidin, the reductions in effective ionic diffusion coefficients observed here are generally smaller, though as was discussed above, the effective diffusion coefficient that was being considered in most of that work was that for crossing a fixed free-energy barrier due to the protein potential, whereas here we are more concerned with the effect of the water on the ion. The simulations on gramicidin, compared more fully in Roux and Karplus (1991a), give results for D of sodium between 0.058 Å^2 ps^{-1} and 5×10^{-4} Å^2 ps^{-1}, compared with an estimated experimental value (folding in the effects of barrier crossings and access resistance) of 9×10^{-4} Å^2 ps^{-1}. It is interesting that the nature of the ionic motions considered here, in these somewhat larger channels, is simpler to study than in gramicidin, where the very intimate ion-pore interactions accurate and time-consuming free energy perturbation and activated dynamics calculations

(Roux and Karplus, 1991b; Roux and Karplus, 1994; Roux, 1995). In the present studies, details of the simulation technique—for example the type of restraints placed on the channel protein—seem less critical than was the case in gramicidin. Aside from the studies on gramicidin and the work of Lynden-Bell and Rasaiah, other estimates of D of ions in channels have tended to come from fitting theoretical results to experimental I-V curves and permeability ratios. For example, in Chen et al. (1997a), ionic diffusion coefficients and other parameters are fitted using the Poisson-Nernst-Planck equation to a large amount of current-voltage data for the same leu-ser peptide as was studied here.

Thus, it seems to be empirically the case that D of an ion in a channel is influenced to a large extent by the effects of confinement; though potential wells and barriers will have a dominant effect on diffusion through the channel as a whole and must be included in conductance calculations, their effect on the short-range motions considered here seems to be relatively small, unless the field is very large (e.g., near charged sidechains or the helix termini of narrow channels). In this case, it is difficult to disentangle the effects of the field from a true variation in D.

As we have said, we believe that the diffusion coefficients measured empirically here will be useful in the coarse-grained methods of calculating channel conductance mentioned in the introduction. For example, perhaps the commonest approach to conductance calculations is the Nernst-Planck equation:

$$\boldsymbol{J} = -\sum_i D_i(c_i \nabla\Phi + \nabla c_i) \qquad (5)$$

where Φ is the electrostatic energy of the ion in temperature units, related to the conventional electrostatic potential ϕ (in volts) by $\Phi = Z_i F\phi/RT$, with T temperature and Z ionic valence. c is the ionic concentration, D is the diffusion coefficient (which may vary spatially), and the subscript i labels the different ionic species in the system. The boundary conditions that produce the flux are the values of ϕ and c at the two ends of the channel. It is usual to consider the problem as effectively one-dimensional, so that $\nabla \rightarrow d/dz$. Methods based on this, but differing in their treatment of ion-ion interactions, have been used on several channel models (Kienker and Lear, 1995; Woolley et al., 1997; Chen et al., 1997a; Chen et al., 1997b). The effective diffusion constant D in all these methods acts as a constant of proportionality, relating the size of the response (current density) to the effective force $c_i\nabla\Phi + \nabla c_i$. Thus, to a first approximation, a reduction in D due to confinement in the channel will produce a proportionate reduction in J and thus in the single-channel conductance. It plays a similar role in other techniques such as Eyring Rate Theory (Cooper et al., 1985), Brownian Dynamics (Cooper et al., 1985), and Langevin Dynamics simulation (Binney et al., 1992; Li et al., 1998). A good comparative overview of such coarse-grained models appears in Cooper et al. (1985). We remark in this connection that in obtaining the electrical potential ϕ from the Poisson equation, it is important to consider that a reduction in the effective dielectric constant ϵ of pore water may also occur in channels composed of α-helix bundles, due to alignment of water by the helix dipole fields (Sansom et al., 1997).

CONCLUSION

The diffusion coefficient of sodium ions in models of ion channels was found to be reduced relative to bulk solution. The extent of this reduction depends on the radius of the channel and is greatest for narrow channels; in the an5 model (a pentameric bundle of poly-alanine α-helices) it is reduced approximately tenfold, and even near the center of a wide pore, like that of the nicotinic acetylcholine receptor, it seems to be about 30% less on average than in bulk solution. This is consistent with previous studies on cylindrical hydrophobic cavities (Lynden-Bell and Rasaiah, 1996). There is some evidence that $D_{\|}$ is reduced less than $D_{\perp}$, particularly near the mouths of channels. Moreover, D seems to be reduced still further near the protein surface of the nicotinic receptor. This behavior may reduce the effective radius of the channel, though in this case the local electric fields are very strong and it is difficult to separate effects of D from those caused directly by the field.

The existence and size of the reduction in D does not seem to depend on whether the channel is a helix bundle or a β-barrel; the radius is the primary determinant. However, direct interactions between the ion and channel sidechain atoms are more important in channels with a hydrophilic lining than in hydrophobic channels, an observation which has implications for ion selectivity.

The diffusion coefficients of ions in channels make up one group of parameters that can be determined by MD simulation and then used in coarse-grained simulation or differential equation-based techniques (Cooper et al., 1985; Chen et al., 1997a; Kuyucak et al., 1998) for finding channel conductance, thus overcoming the difficulty of reaching physiological timescales with MD simulations alone. Further work will attempt to refine the diffusion coefficients measured here, to separate more clearly the free energy barriers due to water from those due to protein, and to extend the measurements to other physiologically important ions such as K^+ and Cl^-, as well as using the diffusion constants in conductance calculations.

APPENDIX A
Rare Large Jumps in the an5 Model: A Bayesian Approach

In the case of the an5 channel the ion trajectory seemed to show a different kind of diffusion from that seen in the other channels; the ion was almost stationary in z for long periods, but made occasional large jumps of roughly constant size, approximately 2 Å. The number of such jumps during a particular trajectory was small. It is not clear that Eq. 1 is still appropriate

to analyze this motion, so we have compared the results of Eq. 1 with those of the following different approach.

We have a one-dimensional problem of hopping on a lattice. If the time of observation is T, and the distance jumped (lattice spacing) is a, then the probability of observing N jumps by the ion, given that the diffusion coefficient is in reality D and the jumps are independent, is given by the Poisson distribution:

$$P(N|D) = \frac{1}{N!}(2DT/a^2)^N e^{-2DT/a^2}$$

Now Bayes' theorem (Bretthorst, 1990; Loredo, 1990) can be used to invert this to give the probability that the diffusion coefficient is in reality D, given that N jumps were observed:

$$P(D|N) = \frac{P_{\text{prior}}(D)P(N|D)}{\int_{-\infty}^{\infty} P_{\text{prior}}(D)P(N|D)dD} \quad (6)$$

$P_{\text{prior}}(D)$ is the prior probability of D, i.e., the probability distribution assigned to D before taking the data into account. We choose the simple (unnormalized) prior probability

$$P_{\text{prior}}(D) = \begin{cases} 0 & \text{if } D < 0 \\ 1 & \text{if } D \geq 0 \end{cases}$$

This accounts for the fact that D cannot be negative, but otherwise says nothing about it. The precise form of the prior probability typically has little effect, unless N is very small. Substituting $P_{\text{prior}}(D)$ into Eq. 6 has the effect merely of changing the lower limit of integration from $-\infty$ to 0. Putting in the expression for $P(N|D)$ we finally obtain

$$P(D|N) = D^N(2T/a^2)^{N+1}e^{-DT/a^2} \quad (7)$$

for $D \geq 0$, and $P(D) = 0$ otherwise. From this it follows that

$$\langle D \rangle = \int_0^{\infty} DP(D|N)dD = \frac{a^2(N+1)}{2T} \quad (8)$$

and

$$\text{var}(D) = \frac{a^4(N+1)}{4T^2} \quad (9)$$

It should be noted that this does not reduce to $\langle D \rangle = 0$ if $N = 0$, but to a^2T. This sort of behavior is characteristic of Bayesian methods, which give a finite probability to a nonzero D even if no transitions are observed; $\langle D \rangle$ decreases as the observation time increases. It should be noted, however, that Eq. 7 shows that 0 is the most probable value of D in this case. We use $\langle D \rangle$ as our best estimator of D.

APPENDIX B
Investigation of the Simulation Protocol

In this appendix we describe the tests that were done during development of the simulation procedure used to produce the results described above. The tests were performed on the n8s8 and an5 models and the (31 Å)^3 water box. The factors investigated were the choice of thermodynamic ensemble (constant energy, NVE, the usual MD choice, or constant temperature, NVT, implemented with the Nosé-Hoover method), choice of electrostatic truncation (cutoff with force-shift or extended electrostatics) (Stote et al., 1991), and choice of either reflecting (implemented with MMFP) or periodic boundary conditions. In the case of an5 we also investigated the effect of replacing the Cα restraints with harmonic restraints between adjacent helices, which allow greater flexibility in the channel (simulations performed with restraints between helices are marked with *). The results are shown in Table 1. Generally, the protocol does not seem to affect the results within the error bars, providing further evidence in support of the use of the Cα restraints.

TABLE 1 Tests of simulation procedures

Model	Ensemble	Electrostatics	D/Å^{2}ps^{-1}
water box	nve	Cutoff, pbc	0.13 (6)
an5	nvt	Extended	0.02 (2) ($z = 0$)
	nvt	Cutoff*	0.02 (2) ($z = 0$)
			0.06 (4) ($z = -5$)
	nvt	Cutoff**	0.03 (2) ($z = 0$)
n8s8	nve	Cutoff	0.04 (3) ($z = 0$)
	nvt	Cutoff**	0.03 (2) ($z = 5$)

nve, thermodynamic ensemble with constant number of particles, volume, and energy; nvt, thermodynamic ensemble with constant number of particles, volume, and temperature; pbc, periodic boundary conditions; *, simulation was performed with interhelix structural restraints instead of Cα restraints; **, ion was not restrained during minimization and heating.

We decided to use the constant-NVT ensemble for its slightly greater physical realism and cutoff electrostatics for computational cheapness. Another result of these simulations was introduction of the mmfp restraint that held the ion near its starting point during minimization and heating. Initially it was not included (simulations marked ** were done without it), but we found that if it was not present, the ion tended to move a long way during the minimization and heating stages, and so its movements during the production stage did not then always provide a measure of D in the vicinity of its starting point, as desired.

This work was supported by a grant from the Wellcome Trust. We thank the Oxford Centre for Molecular Sciences for the use of computing facilities.

REFERENCES

Adcock, C., G. R. Smith, and M. S. P. Sansom. 1998. Electrostatistics and the ion selectivity of ligand-gated channels. *Biophys. J.* 75:1211–1222.

Akabas, M. H., C. Kaufmann, T. A. Cook, and P. Archdeacon. 1994. Amino acid residues lining the chloride channel of the cystic fibrosis transmembrane conductance regulator. *J. Biol. Chem.* 269: 14865–14868.

Akabas, M. H., D. A. Stauffer, M. Xu, and A. Karlin. 1992. Acetylcholine receptor channel structure probed in cysteine-substitution mutants. *Science.* 258:307–310.

Alder, B. J., and T. Wainwright. 1970. Decay of the velocity autocorrelation function. *Phys. Rev. A.* 1:18–21.

Allen, M. P., and D. J. Tildesley. 1987. Computer Simulation of Liquids. Clarendon Press, Oxford.

Berne, B. J. 1985. Molecular dynamics and Monte Carlo simulations of rare events. *In* Multiple Time Scales. Academic Press, New York. 419–436.

Bertrand, D., A. Devillers-Thiéry, F. Revah, J. L. Galzi, N. Hussy, C. Mulle, S. Bertrand, M. Ballivet, and J.-P. Changeux. 1992. Unconventional pharmacology of a neuronal nicotinic receptor mutated in the channel domain. *Proc. Natl. Acad. Sci. USA.* 89:1261–1265.

Binney, J. J., N. J. Dowrick, A. J. Fisher, and M. E. J. Newman. 1992. The Theory of Critical Phenomena: An Introduction to the Renormalization Group. Clarendon Press, Oxford.

Breed, J., P. C. Biggin, I. D. Kerr, O. S. Smart, and M. S. P. Sansom. 1997. Alamethicin channels: modelling via restrained molecular dynamics simulations. *Biochim. Biophys. Acta.* 1325:235–249.

Breed, J., R. Sankararamakrishnan, I. D. Kerr, and M. S. P. Sansom. 1996. Molecular dynamics simulations of water within models of ion channels. *Biophys. J.* 70:1643–1661.

Bretthorst, G. L. 1990. An introduction to parameter estimation using Bayesian probability theory. *In* Maximum Entropy and Bayesian Meth-

ods, P. F. Fougère, editor. Kluwer Acad. Publ., Dordrecht, The Netherlands. 53–79.

Brooks, B. R., R. E. Bruccoleri, B. D. Olafson, D. J. States, S. Swaminathan, and M. Karplus. 1983. CHARMM: a program for macromolecular energy, minimisation, and dynamics calculations. *J. Comp. Chem.* 4:187–217.

Cafiso, D. S. 1994. Alamethicin: a peptide model for voltage gating and protein-membrane interactions. *Annu. Rev. Biophys. Biomol. Struct.* 23:141–165.

Changeux, J. P., J. I. Galzi, A. Devillers-Thiéry, and D. Bertrand. 1992. The functional architecture of the acetylcholine nicotinic receptor explored by affinity labelling and site-directed mutagenesis. *Quart. Rev. Biophys.* 25:395–432.

Chen, D., J. Lear, and R. S. Eisenberg. 1997a. Permeation through an open channel: Poisson-Nernst-Planck theory of a synthetic ion channel. *Biophys. J.* 72:92–116.

Chen, D., L. Xu, A. Tripathy, G. Meissener, and R. S. Eisenberg. 1997b. Permeation through the calcium release channel of cardiac muscle. *Biophys. J.* 73:1337–1354.

Chiu, S.-W., and E. Jakobsson. 1989. Stochastic theory of singly occupied ion channels II: effects of access resistance and potential gradients extending into the bath. *Biophys. J.* 55:147–157.

Chiu, S.-W., E. Jakobsson, S. Subramaniam, and J. A. McCammon. 1991. Time-correlation analysis of simulated water motion in flexible and rigid gramicidin channels. *Biophys. J.* 60:273–285.

Chiu, S.-W., J. A. Novotny, and E. Jakobsson. 1993. The nature of ion and water barrier crossings in a simulated ion channel. *Biophys. J.* 64: 98–108.

Cohen, B. N., C. Labarca, L. Czyzyk, N. Davidson, and H. A. Lester. 1992. $Tris^+/Na^+$ permeability ratios of nicotinic acetylcholine receptors are reduced by mutations near the intracellular end of the M2 region. *J. Gen. Physiol.* 99:545–572.

Cohen, E. G. D. 1993. Fifty years of kinetic theory. *Physica A*. 194: 229–257.

Cooper, K., E. Jakobsson, and P. Wolynes. 1985. The theory of ion transport through membrane channels. *Prog. Biophys. Molec. Biol.* 46: 51–96.

Cowan, S. W., T. Schirmer, G. Rummel, M. Steiert, R. Ghosh, R. A. Apuptit, J. N. Jansonius, and J. P. Rosenbusch. 1992. Crystal structures explain functional properties of two *E. coli* porins. *Nature.* 358:727–733.

Doyle, D. A., J. M. Cabral, R. A. Pfuetzner, A. Kuo, J. M. Gulbis, S. L. Cohen, B. T. Chait, and R. Mackinnon. 1998. The structure of the potassium channel: Molecular basis of K^+ conduction and selectivity. *Science.* 280:69–77.

Doyle, D. A., and B. A. Wallace. 1997. Crystal structure of the gramicidin/potassium thiocyanate complex. *J. Mol. Biol.* 266:963–977.

Dwyer, T. M., D. J. Adams, and B. Hille. 1980. The permeability of the endplate channel to organic cations in frog muscle. *J. Gen. Physiol.* 75:469–492.

Fox, R. O., and F. M. Richards. 1982. A voltage-gated ion channel model inferred from the crystal structure of alamethicin at 1.5 resolution. *Nature.* 300:325–330.

Galzi, J. L., A. Devillers-Thiéry, N. Hussy, S. Bertrand, J.-P. Changeux, and D. Bertrand. 1992. Mutations in the channel domain of a neuronal nicotinic receptor convert ion selectivity from cationic to anionic. *Nature.* 359:500–505.

Grey, H. L., and W. R. Schucany. 1972. The Generalized Jackknife Statistic. M. Dekker, New York.

Gutman, M., A. Tsfadia, A. Masad, and E. Nachiel. 1992. Quantitation of physical-chemical properties of the aqueous phase inside the PhoE ionic channel. *Biochem. Biophys. Acta.* 1109:141–148.

Hille, B. 1992. Ionic Channels of Excitable Membranes, 2nd ed. Sinauer Associates Inc., Sunderland, Mass.

Hucho, F., W. Oberthr, and F. Lottspeich. 1986. The ion channel of the nicotinic acetylcholine receptor is formed by the homologous helices M II of the receptor subunits. *FEBS Lett.* 205:137–142.

Hucho, F., V. Tsetlin, and J. Machold. 1996. The emerging three-dimensional structure of a receptor: The nicotinic acetylcholine receptor. *Eur. J. Biochem.* 239:539–557.

Jakobsson, E., and S.-W. Chiu. 1987. Stochastic theory of ion movement in channels with single-ion occupancy: Application to sodium permeation of gramicidin channels. *Biophys. J.* 52:33–45.

Jordan, P. C. 1982. Electrostatic modeling of ion pores. Energy barriers and electric field profiles. *Biophys. J.* 39:157–164.

Karlin, A., and M. H. Akabas. 1995. Towards a structural basis for the function of nicotinic acetylcholine receptors and their cousins. *Neuron.* 15:1231–1244.

Keizer, J. 1987. Statistical Thermodynamics of Non-equilibrium Processes. Springer-Verlag, New York.

Kerr, I. D., R. Sankararamakrishnan, O. S. Smart, and M. S. P. Sansom. 1994. Parallel helix bundles and ion channels: molecular modelling via simulated annealing and restrained molecular dynamics. *Biophys. J.* 67:1501–1515.

Kienker, P. K., W. F. DeGrado, and J. D. Lear. 1994. A helical-dipole model describes the single-channel current rectification of an uncharged peptide ion channel. *Proc. Natl. Acad. Sci. USA.* 91:4859–4863.

Kienker, P. K., and J. D. Lear. 1995. Charge selectivity of the designed uncharged peptide ion channel. Ac-$(LSSLLSL)_3$-$CONH_2$. *Biophys. J.* 68:1347–1358.

Kraulis, P. J. 1991. MOLSCRIPT: a program to produce both detailed and schematic plots of protein structures. *J. Appl. Cryst.* 24:946–950.

Kreusch, A., A. Neubueser, W. Schiltz, J. Wekesser, and G. E. Schulz. 1994. The structure of the membrane channel porin from *Rhodopseudomonas blastica* at 2.0 Å resolution. *Protein Sci.* 3:58–63.

Kuyucak, S., M. Hoyles, and S.-H. Chung. 1998. Analytical solutions of Poisson's equation for realistic geometrical shapes of membrane ion channels. *Biophys. J.* 74:22–36.

Lear, J. D., Z. R. Wasserman, and W. F. DeGrado. 1988. Synthetic amphiphilic peptide models for protein ion channels. *Science.* 240: 1177–1181.

Lear, J. D., Z. R. Wasserman, and W. F. DeGrado. 1994. Use of synthetic peptides for the study of membrane protein structure. *In* Membrane Protein Structure, Stephen H. White, editor. Oxford University Press, New York. 335–354.

Li, S. C., M. Hoyles, S. Kuyucak, and S.-H. Chung. 1998. Brownian dynamics study of ion transport in the vestibule of membrane channels. *Biophys. J.* 74:37–47.

Loredo, T. J. 1990. From Laplace to supernova SN1987A: Bayesian inference in astrophysics. *In* Maximum Entropy and Bayesian Methods, P. F. Fougère, editor. Kluwer Academic Publishing, Dordrecht, The Netherlands.

Lynden-Bell, R. M., and J. C. Rasaiah. 1996. Mobility and solvation of ions in channels. *J. Chem. Phys.* 105:9266–9280.

Mitton, P., and M. S. P. Sansom. 1996. Molecular dynamics simulations of ion channels formed by bundles of amphipathic α-helical peptides. *Eur. Biophys. J.* 25:139–150.

Nicholson, L. K., Q. Teng, and T. A. Cross. 1991. Solid-state nuclear magnetic resonance derived model for dynamics in the polypeptide backbone of the gramicidin A channel. *J. Mol. Biol.* 218:621–637.

Nosé, S. 1984. A molecular dynamics method for simulations in the canonical ensemble. *Mol. Phys.* 53:255–268.

Nutter, T. J., and D. J. Adams. 1995. Monovalent and divalent cation permeability and block of neuronal nicotinic receptor channels in rat parasympathetic ganglia. *J. Gen. Physiol.* 105:701–723.

Ortells, M. O., and G. G. Lunt. 1996. A mixed helix-beta-sheet model of the transmembrane region of the nicotinic acetylcholine receptor. *Protein Eng.* 9:51–59.

Roux, B. 1995. Theory of transport in ion channels. *In* Computer Modelling in Molecular Biology, J. M. Goodfellow, editor. VCH Verlagsgesellschaft, Weinheim, Germany. 134–169.

Roux, B., and M. Karplus. 1991a. Ion transport in a gramicidin-like channel: dynamics and mobility. *J. Phys. Chem.* 95:4856–4868.

Roux, B., and M. Karplus. 1991b. Ion transport in a model gramicidin channel: structure and thermodynamics. *Biophys. J.* 59:961–981.

Roux, B., and M. Karplus. 1993. Ion transport in the gramicidin channel: free energy of the solvated right-handed dimer in a model membrane. *J. Am. Chem. Soc.* 115:3250–3262.

Roux, B., and M. Karplus. 1994. Molecular dynamics simulations of the gramicidin channel. *Annu. Rev. Biophys. Biomol. Struct.* 23:731–761.

Roux, B., B. Prod'hom, and M. Karplus. 1995. Ion transport in the gramicidin channel: molecular dynamics study of single and double occupancy. *Biophys. J.* 68:876–892.

Sancho, M., M. B. Partenskii, V. Dorman, and P. C. Jordan. 1995. Extended dipolar chain model for ion channels: electrostatic effects and the translocational energy barrier. *Biophys. J.* 68:427–433.

Sankararamakrishnan, R., C. Adcock, and M. S. P. Sansom. 1996. The pore domain of the nicotinic acetylcholine receptor: molecular modelling, pore dimensions and electrostatics. *Biophys. J.* 71:1659–1671.

Sansom, M. S. P. 1993. Structure and function of channel-forming peptaibols. *Quart. Rev. Biophys.* 26:365–421.

Sansom, M. S. P., R. Sankararamakrishnan, and I. D. Kerr. 1995. Modelling membrane proteins using structural restraints. *Nature Struct. Biol.* 2:624–631.

Sansom, M. S. P., G. R. Smith, C. Adcock, and P. C. Biggin. 1997. The dielectric properties of water within model transbilayer pores. *Biophys. J.* 73:2404–2415.

Skerra, A., and J. Brickmann. 1987. Simulation of voltage-driven hydrated cation transport through narrow transmembrane channels. *Biophys. J.* 51:977–983.

Smart, O. S., J. Breed, G. R. Smith, and M. S. P. Sansom. 1997. A novel method for structure-based prediction of ion channel conductance properties. *Biophys. J.* 72:1109–1126.

Smart, O. S., J. M. Goodfellow, and B. A. Wallace. 1993. The pore dimensions of gramicidin A. *Biophys. J.* 65:2455–2460.

Smith, G. R., and M. S. P. Sansom. 1997. Molecular dynamics study of water and Na^+ ions in the pore region of the nicotinic acetylcholine receptor. *Biophys. J.* 73:1364–1381.

Song, L., M. R. Hobaugh, C. Shustak, S. Cheley, H. Bayley, and J. E. Gouaux. 1996. Structure of staphyloccal α-hemolysin, a heptameric transmembrane pore. *Science.* 274:1859–1866.

Stote, R. H., D. J. States, and M. Karplus. 1991. On the treatment of electrostatic interactions in biomolecular simulation. *J. Chim. Phys.* 88:2419–2433.

Tikhonov, D. B., and B. S. Zhorov. 1998. Kinked-helices model of the nicotinic acetylcholine receptor ion channel and its complexes with blockers: simulation by the Monte Carlo minimization method. *Biophys. J.* 74:242–255.

Unwin, N. 1993. Nicotinic acetylcholine receptor at 9 Å resolution. *J. Mol. Biol.* 229:1101–1124.

Unwin, N. 1995. Acetylcholine receptor channel imaged in the open state. *Nature.* 373:37–43.

Urry, D. W. 1971. The gramicidin A transmembrane channel: a proposed $\pi_{(L,D)}$ helix. *Proc. Natl. Acad. Sci. USA.* 68:672–676.

Villarroel, A., S. Herlitze, M. Koenen, and B. Sakmann. 1991. Location of a threonine residue in the α-subunit M2 transmembrane segment that determines the ion flow through the acetylcholine receptor channel. *Proc. R. Soc. Lond. B.* 243:69–74.

Wallace, B. A. 1986. Structure of gramicidin A. *Biophys. J.* 49:295–306.

Woolley, G. A., and B. A. Wallace. 1992. Model ion channels: gramicidin and alamethicin. *J. Membr. Biol.* 129:109–136.

Woolley, G. A., P. C. Biggin, A. Scultz, L. Lien, D. C. J. Jaikaran, J. Breed, K. Crowhurst, and M. S. P. Sansom. 1997. Intrinsic rectification of ion flux in alamethicin channels: studies with an alamethicin dimer. *Biophys. J.* 73:770–778.

You, S., S. Peng, L. Lien, J. Breed, M. S. P. Sansom, and G. A. Woolley. 1996. Engineering stabilized ion channels: covalent dimers of alamethicin. *Biochemistry.* 35:6225–6232.

Zhong, Q., Q. Jiang, P. B. Moore, D. M. Newns, and M. L. Klein. 1998. Molecular dynamics simulation of a synthetic ion channel. *Biophys. J.* 74:3–10.